Physics Letters B 838 (2023) 137717

Contents lists available at ScienceDirect

Physics Letters B

journal homepage: www.elsevier.com/locate/physletb

Quantifying the second resonance effect in neutrino-Argon interaction using DUNE Near Detector

R Lalnuntluanga *, A Giri

Department of Physics, Indian Institute of Technology Hyderabad, Kandi, Hyderabad, 502284, Telangana, India

ARTICLE INFO

Article history:
Received 2 August 2022
Received in revised form 19 January 2023
Accepted 19 January 2023
Available online 23 January 2023
Editor: B. Balantekin

Keywords:
Neutrino interaction
Monte Carlo simulation

ABSTRACT

Heavy nuclear targets are used in neutrino oscillation experiments to boost the statistics of neutrino interactions. The complex nuclear environment contributes to the systematic uncertainty as the inevitable nuclear effects. Inadequate knowledge of the neutrino interaction with the nuclear target along with the imperfect reconstruction of neutrino energy seeds uncertainty in the cross-section. Uncertainty in the cross-section propagates as a systematic uncertainty in the determination of the neutrino oscillation parameters. For precision physics, future neutrino oscillation experiments will require understanding of the neutrino nucleus-interaction and neutrino energy reconstruction with a high level of accuracy. In this work, we aim to quantify the second resonance contributions to the neutrino interaction in Argon for reducing systematic uncertainties in the physics predictions for the DUNE Near Detector (ND). We present the results as the ratio distribution of $\frac{d\sigma}{dQ^2}$ for $\Delta(1232)$ resonance and the extended analysis to the second resonance region $P_{11}(1440)$, $D_{13}(1520)$, and $S_{11}(1535)$. This inclusion shows a significant contribution to the total cross-section compared to the case where only the $\Delta(1232)$ resonance is considered.

1. Introduction

The current goals of the ongoing neutrino oscillation experiments such as, NOνA [1], T2K [2], and future experiments such as, DUNE [3], and Hyper-Kamiokande [4] are to precisely determine the parameters of neutrino oscillations and for the better understanding of the neutrino interaction with nucleus. Since the oscillation probabilities depend on the neutrino energy it is very essential to reconstruct the neutrino energy accurately. The neutrino beams produced by the decay of mesons (π, K) at accelerator facilities present a broad energy spectrum. Moreover, the neutrino energy needs to be reconstructed on an event-by-event basis from the particles obtained in the final states. Needless to mention, understanding of the neutrino-nucleus interactions is vital for the precise reconstruction of neutrino energy. The environment of the nucleus also alters the particles produced in the initial neutrino nucleon interaction vertex and the kinematics of the interaction. These ineluctable nuclear effects result in mis-characterizing the final state particles, and inaccurate reconstruction of neutrino energy. Identification of nuclear effects in neutrino-nucleus interactions is desirable along with the difference in neutrino and anti-neutrino scattering cross-sections. Many long-baseline neutrino experiments use heavy nuclear targets, such as Argon [5,6], Oxygen [7], Water [8], and Iron [9,10] to obtain larger interaction rates than those of thin targets, such as Hydrogen, and Deuterium, which are limited by statistics. Our limited knowledge of nuclear effects results in additional systematic uncertainties. Understanding the interplay between neutrino-nucleus cross-sections and nuclear effects is also essential for the precision determination of neutrino oscillation parameters. Precision measurements of neutrino oscillation experiments require understanding of the cross-sections in neutrino-nucleus interaction as they aid us in improving the neutrino event generator.

The neutrino interaction is complicated due to differences in the physics mechanism and overlaps of many interaction channels such as Quasi-Elastic (QE), Resonance (RES), the non-resonant process called Deep Inelastic Scattering (DIS), and Coherent Scattering (COH), etc. The presence of the multinucleon events also complicates the few-GeV energy region which can appear as fake QE events, as it can have the same experimental signature as a true QE ($1\mu^-$, 0π) [11]. In this process, the neutrino interacts with a correlated pair of nucleons and results in the ejection of two nucleons from the nucleus. Therefore, multi-nucleon events are identified as multiple nucleons in the final state. $2p2h$ is the dominant contribution to these events and their importance for future experiments, such as DUNE, is studied here [12]. The pions produced

* Corresponding author.
E-mail address: ph19resch11003@iith.ac.in (R Lalnuntluanga).

https://doi.org/10.1016/j.physletb.2023.137717

through the RES processes can be altered in the nuclear medium of the target which constitutes the major background for the QE process. The cross-section of the RES process needs to be understood with high accuracy, and concurrently identified and distinct the COH component.

Neutrino scattering interactions are simulated using Monte Carlo (MC) event generators, which are developed by theoretical communities using different nuclear models. MC generators are essential tools, as they serve as a bridge for the theoretical and experimental communities. They are used to predict and make improvements for future experiments. The widely used event generators are GENIE [13], GiBUU [14], NuWro [15] and NEUT [16]. GENIE is currently used as the primary generator by Fermilab experiments such as NOνA, MINERνA [17], SBN [18], DUNE, while NEUT is currently employed by T2K, Super-Kamiokande [19], and Hyper-Kamiokande. GiBUU and NuWro are theory-oriented generators, often used as additional points of references. Neutrino-nucleus interaction events predicted by these generators depend on the theoretical models, any mis-modeling would enhance large uncertainties in the predicted event rate and the final state particle topology. It is important to have a good understanding of the neutrino-nucleus cross-section and the nuclear effects in order to achieve high precision neutrino physics.

This article presents a simulation-based analysis using GENIE-3.00.06 (tune G18_10a_02_11a) [13] and GiBUU-2021 [14] for the DUNE ND High-Pressure gas Time Projection Chamber (HpgTPC) [20] to quantify the effect of the second resonance region [21], induced by the charge current (anti)neutrino interaction in the Argon target. Previous studies show a small amount of contribution from the second resonance cross-section using the Carbon target, which is non-negligible [22,23]. More studies on the second resonance region can be found here [24–26]. With the need to achieve the required precision for future neutrino experiments such as DUNE, it will be important to understand the effect of the second resonance in the Argon target as hinted here [27]. We present our results for the flux-integrated differential cross-section as a function of Q^2-squared four-momentum transfer for Argon and Carbon targets.

This paper is organized as follows: In Section 2, we describe the framework with a detailed description of the Monte Carlo event generator used, the formalism for the neutrino interaction, and the neutrino energy reconstruction. The simulation and experimental details of HpgTPC and its particle detection threshold are mentioned in Section 3. The results obtained from our analysis are presented in Section 4 and conclusions are discussed in Section 5.

2. Framework

2.1. Monte Carlo event generator : GENIE and GiBUU

In this article, both the neutrino cross-sections and interaction are simulated using GENIE [13] and GiBUU [14]. GENIE is widely used by major neutrino accelerator experiments such as MINERνA [17], MINOS [28], MicroBooNE [29], NOνA [1], LBNE [30] and is also used by T2K [2] experiment. GiBUU has been used broadly to determine the nuclear effects which plays significant roles in experimental analyses.

In GENIE, the nuclear ground state is described by the Relativistic Fermi Gas model [31]. The GENIE implementation of the Local Fermi Gas (LFG) to explain the nuclear ground state is considered in the simulation. The nucleons populate all the momentum states up to the global Fermi momentum with equal probability in the case of regular Fermi Gas. In the LFG model, the Fermi momentum relies on the local nuclear density which varies with the radial position. In GiBUU, a density dependent mean-field potential term is added to the Fermi Gas model where all the nucleons are presumed to be bounded.

The QE scattering and the MEC/2p2h processes are modeled in GENIE using the new models from the Valenica group [32–34]. The QE scattering is modeled using Llewellyn-Smith model [35] which is the default in GiBUU. The detailed description of the implementation of the MEC/2p2h model in GiBUU can be found in Ref. [36]. We consider the value of the charge current QE axial mass $M_A \approx 0.96$ GeV/c^2 [13] in GENIE and 1.0 GeV/c^2 in GiBUU and the vector form factor is defined using BBA05 [37] and BBA07 [38], respectively. Other meson exchange current (MEC)/2p2h model such as Empirical MEC [39] is also available in GENIE. The Berger-Sehgal (BS) model [40], which is similar to the old Rein-Sehgal (RS) model [41], is used for modeling the interactions associated with the baryonic resonances in the neutral current and charge current interactions. Here we consider 16 resonances but neglect the interference between them. The BS model differs from the RS model as the lepton mass effect is included in the former model. The resonances decay isotropically in their center of mass frame given by default. On the other hand, GiBUU consists of 13 kinds of resonance modes where the vector form factors are obtained from the electron scattering data of the MAID analysis [42]. The default value for the resonance axial-vector mass, $M_A^{RES} = 1.12$ GeV/c^2 [43], is considered in GENIE. Other resonant pion production model such as Kuzmin-Lyubushkin-Naumov (KLN) model [44], similar to the RS model, but including the lepton mass effect are also available in GENIE for similar studies. Upcoming GENIE v3 release [45] will include the new resonance single-pion (1π) MK model [46] that completely incorporate the resonance interference effects and the pion angular distribution prediction, which will be studied in the future.

The non-resonant DIS scattering is simulated using Bodek and Yang Model [47] in GENIE while GiBUU uses PYTHIA [48]. An invariant hadronic mass of W $>$ 1.7 GeV cut is applied for bridging the RES and DIS region. For the FSI models, GENIE uses the hA and hN FSI models or the INTRANUKE simulation package [49,50]. The hA model is an empirical data-driven model that uses the cross-sections of pions and nucleons with nuclei for low energies, and CEM03 [51] normalized data for higher energies. While the hN model is a full Intranuclear Nuclear Cascade (INC) model which includes the calculation of nucleons, kaons, pions, and photons' interactions with nuclei energies up to 1.2 GeV. The hA intranuclear cascade model is used in this simulation. The treatment of FSI by GiBUU is quite different from GENIE where the semi-classical BUU equations are solved in which the particle species are coupled by a mean-field potential and collision terms.

2.2. Formalism

Consider CC (anti)neutrino interactions with the nuclear target of mass number A assuming the struck nucleon to be at rest, results in the production of lepton l^- and hadronic final state X given by

$$\nu_l/\bar{\nu}_l + A \rightarrow l^{\mp} + X \tag{1}$$

The hadronic final state X denotes the produced m mesons, the n nucleons knocked-out from the nucleus and the residual $(A-n)$-nucleons. The neutrino energy can be reconstructed from the kinematic variables of the particles in the final state using the kinematic method [52] and the calorimetric method [53]. Using the energy and momentum conservation, the reconstruction of neutrino energy can be calculated from the energy of the particles in the final state [53]

$$E_\nu^{cal} = E_l + \epsilon_n + \sum_i (E_{n_i} - M) + \sum_j E_{m_j} \tag{2}$$

where E_l is the lepton energy, E_{n_i} (M) is the energy (mass) of the i^{th} nucleon with ϵ_n their corresponding separation energies, and E_{m_j} is the energy of the mesons in the final states. This is the calorimetric method and it can be used for any type of CC interaction.

From eqn. (3), it is clear that the neutrino energy is the sum of the observed leptonic and hadronic particles in the final state. So, we can rewrite equation (2) as

$$E_\nu^{cal} = E_l + E_H \tag{3}$$

where,

$$E_H = \sum_i (E_{n_i} - M) + \epsilon_n + \sum_j E_{m_j} \tag{4}$$

Thus, the accuracy of neutrino energy reconstruction heavily relies on accurate reconstruction of the energy accumulated by the baryons and the mesons in the detector. Uncertainties arise in the hadronic energy reconstruction as neutrons escape detection in realistic experiments along with undetected meson which accounted for missing energy [54].

On the other hand, in the kinematic method the neutrino energy can be reconstructed from the kinematics of the final state charged lepton l as [52]

$$E_\nu = \frac{2(M_n - E_b)E_l - (E_b^2 - 2M_n E_b + \Delta M^2)}{2(M_n - E_b - E_l + p_l \cos\theta_l)} \tag{5}$$

where M_n is the rest mass of the free neutron, E_b the binding energy and $\Delta M^2 = M_n^2 - M_p^2 + m_l^2$, with M_p (m_l) the rest mass of the proton (lepton) and $\cos\theta_l$ is the angle between the outgoing lepton and neutrino beam directions. This method is accurate only for the QE interaction. The kinematic method will underestimate the reconstructed energy than expected as it depends only on the lepton's kinematics. The comparison between the kinematic and calorimetric methods for neutrino energy reconstruction has been studied here [53].

The calorimetric method of neutrino energy reconstruction is used in this work. The reconstructed square of the four-momentum transferred from the initial neutrino to the nuclear system is calculated as $Q^2 = 2E_\nu(E_l - p_l\cos\theta_l) - m_l^2$ [55,22]. The formalism for the differential and flux-integrated differential cross-section as a function of Q^2 can be found from reference [23,56–59].

3. Simulation details

This article considers the detection capabilities of particles for the propose DUNE ND HpgTPC [20,60] which uses a mixture of Argon-CH_4 gas with the composition of 90% Argon and 10% CH_4. Most of the interaction will take place with the Argon nuclei (about 97% of the interaction). We have generated 1 million CC-ν_μ and $\bar{\nu_\mu}$ interaction events on Argon and Carbon targets using DUNE ND ($\bar{\nu_\mu}$)ν_μ-flux [61] as shown in Fig. 1, which peaks in the region between 2 and 3 GeV, with the neutrino flux reasonably higher than the anti-neutrino flux. The LBNF (Long-Baseline Neutrino Facility) beamline at Fermilab, an intense (anti)neutrino beam, with an initial beam power of 1.2 MW, with the expectation of 1.1 x 10^{21} protons per year [3]. In the beamline, the high energy protons of 60-120 GeV are produced to smash a graphite target which results in the production of secondary hadrons, mostly pions, and kaons. These secondary particles are then further focused using magnetic horns to the decay pipe (helium filled) where they decay to (anti)neutrino of different types.

The interaction cross-sections computed using GENIE and GiBUU for the charge current ν_μ-Argon (upper panels) and ν_μ-Carbon (lower panels) target as a function of neutrino energy

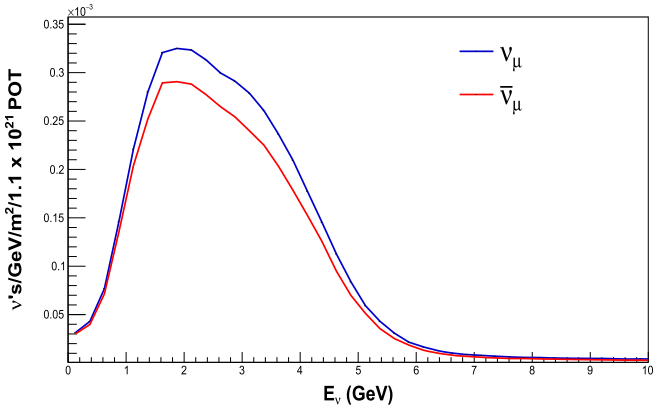

Fig. 1. DUNE (anti)neutrino flux as a function of the neutrino (blue line) and anti-neutrino (red line) energy used in this paper.

is shown in Fig. 2. The variation in the cross-sections for each baryonic resonance can be seen in the figure. The left side is for neutrino mode and the right side is for anti-neutrino mode.

For our analysis, we assume realistic experiments and generate full interaction events which include the Quasi-Elastic (QE), Resonance (RES), two particle-two holes (2p2h/MEC), and Deep Inelastic Scattering (DIS) in neutrino and anti-neutrino mode. In GENIE, the analysis is first done by including only the Δ or $P_{33}(1232)$ excitation of baryonic resonances using the Berger-Seghal model. The analysis is then extended by tuning the Berger-Sehgal cross-section model from the *CommonParam.xml*, where the configuration of the parameters of the cross-section models are defined. We change the parameters of the cross-section model and include the higher order excitation of resonances $P_{11}(1440)$, $D_{13}(1520)$, and $S_{11}(1535)$, i.e., the second resonance region [21]. In GiBUU, the analysis is done using the matrix element from the MAID analysis [42] for the excitation of baryonic resonances, where the module *initNeutrino.f90* gives the calculations of various inclusive neutrino cross sections. We change the module for our analysis to include only the Δ or $P_{33}(1232)$ and the second resonance region ($P_{11}(1440)$, $D_{13}(1520)$, and $S_{11}(1535)$) contribution from the higher order resonance process.

The simulated final state particles are impinged with a realistic experimental kinematic threshold. Due to the limitation of sensitivity in experiments, all the particles that are produced in the interaction are not detected by the detectors. We apply realistic detector cuts of the DUNE ND HpgTPC which have the potential of detecting a pion having a momentum of 5 MeV [62] and a minimum of 3 MeV kinetic energy threshold for protons [3,20]. A kinetic energy cut of 20 MeV for protons with an efficiency of 80% or more has been studied here [12]. A muon having energy 226 MeV (or a momentum cut of 200 MeV) is selected and the kinetic energy cut for neutron varies between 50 MeV to 700 MeV [3]. The distribution of the observed hadronic energy (E_H) in the detector is calculated using equation (4). The reconstructed baryons and mesons in the detector from the Δ-resonance interaction and with the extension to the second resonance region for Argon (upper panel), Carbon (lower panel) using the calorimetric method for GENIE (blue lines), and GiBUU (red lines) are shown in the Fig. 3 for both the neutrino (left) and anti-neutrino (right) mode.

4. Results

From the probability density function (PDF) distribution of the reconstructed hadronic energy shown in the Fig. 3 it can be observed that there is a significant shift in energy distribution for Argon and Carbon targets in both the neutrino and anti-neutrino modes. There is a notable difference for Argon ($\approx$ 130 MeV) and

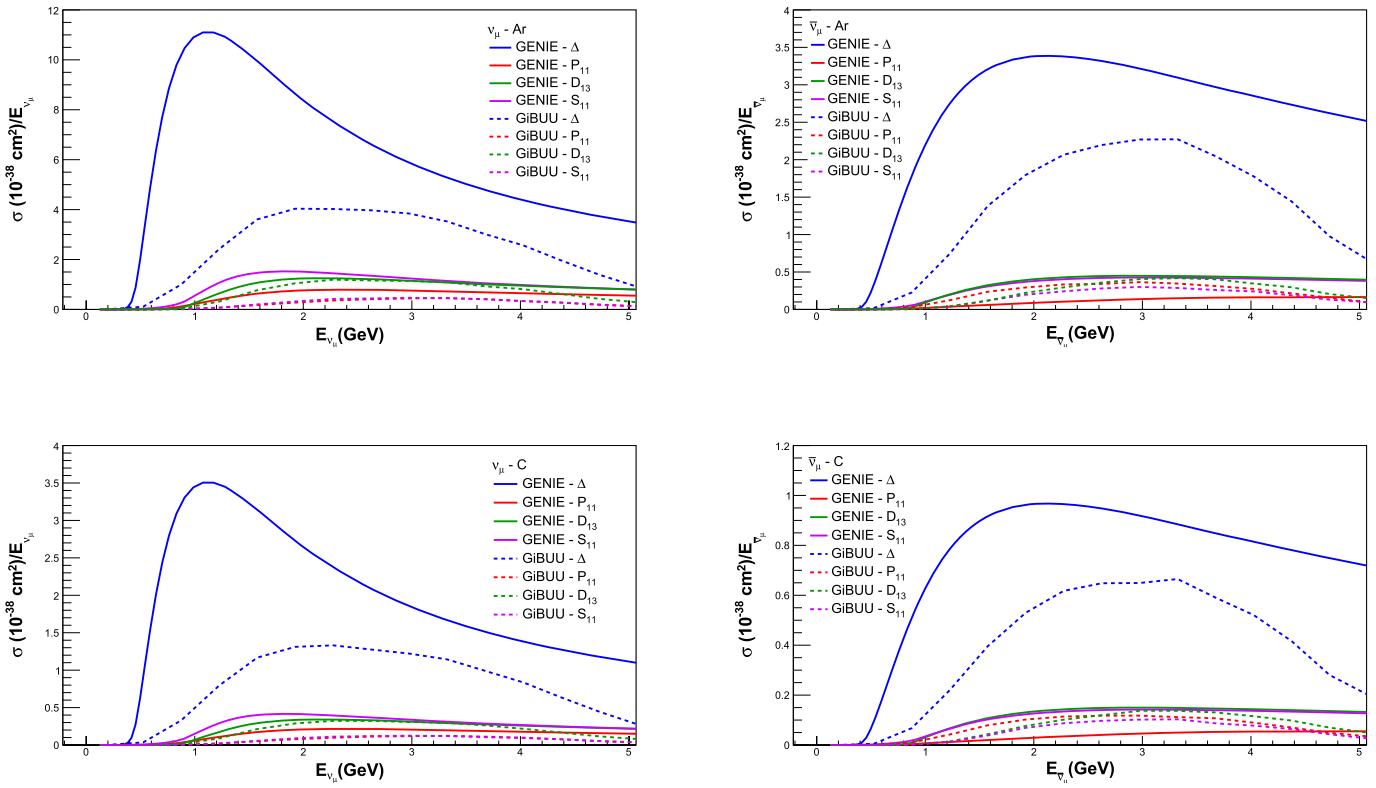

Fig. 2. The plot represents the cross-sections for Δ-resonance (blue) and the second resonance P_{11} (red), D_{13} (green), S_{11} (violet) for Argon (upper panel) and Carbon (lower panel) with neutrino (left) and anti-neutrino (right) using GENIE (solid lines) and GiBUU (dotted lines).

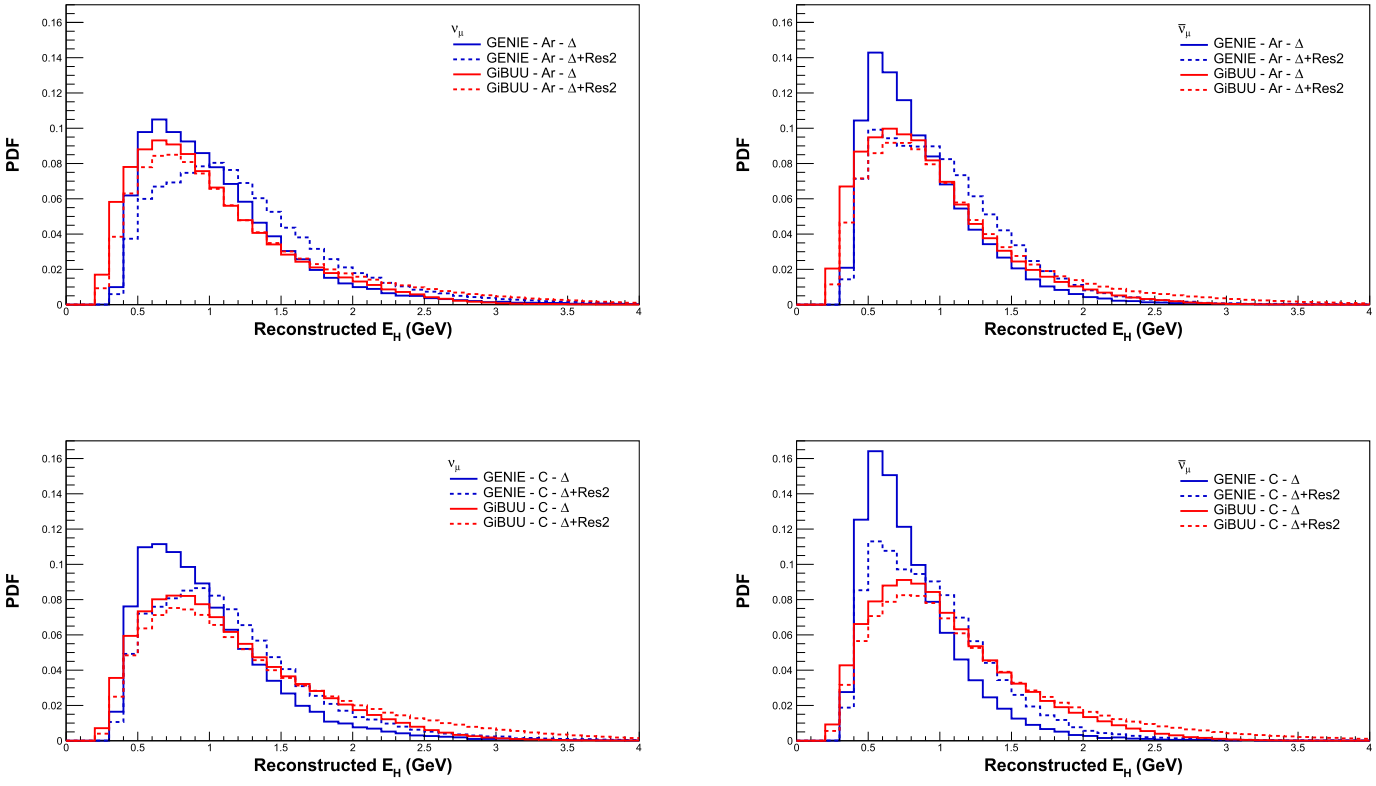

Fig. 3. The plot represents the reconstructed hadronic energy probability density function (PDF) for Δ-resonance (solid lines) and with second resonance i.e. Δ+Res2 (dotted lines) for ν-Argon (upper panel) and ν-Carbon (lower panel) with neutrino (left) and anti-neutrino (right) using GENIE (blue lines) and GiBUU (red lines).

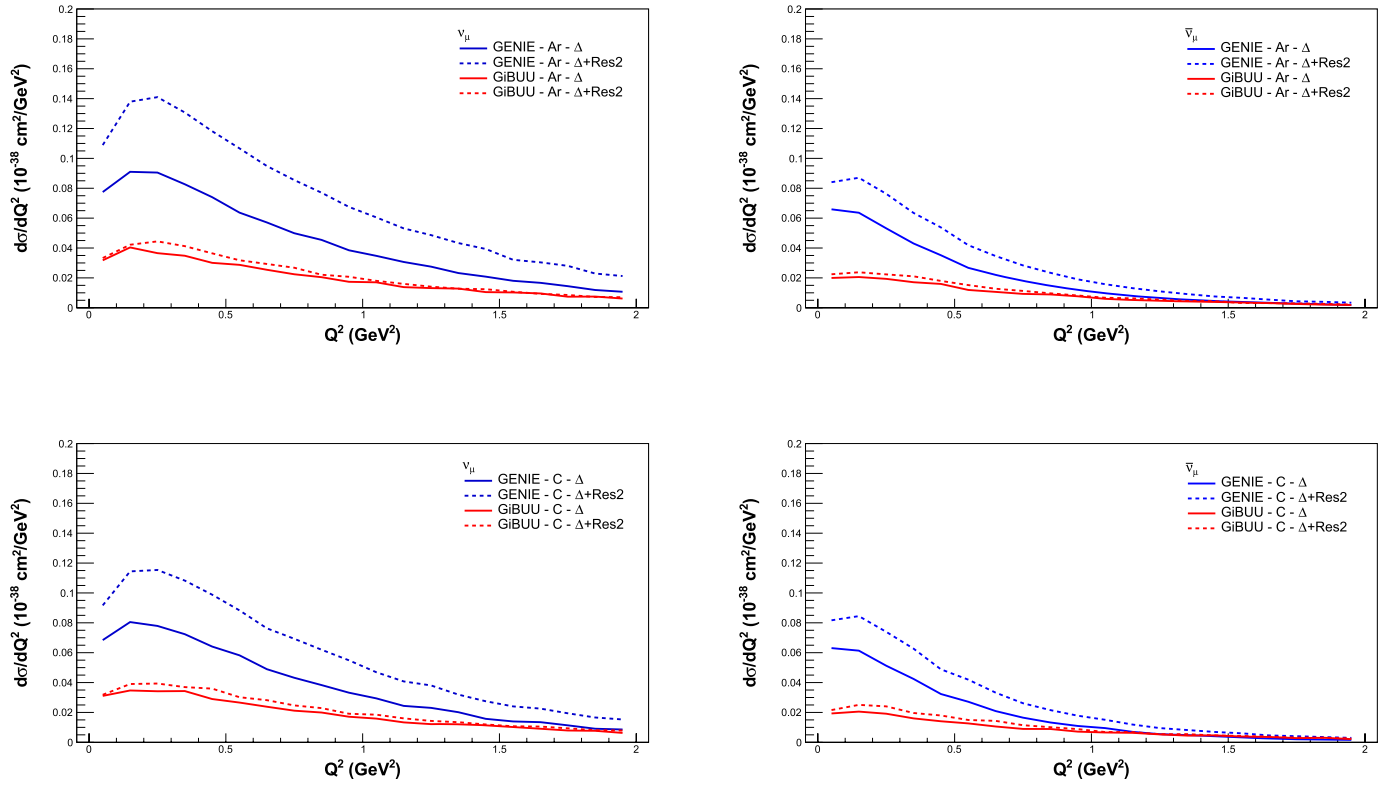

Fig. 4. The plot represents the flux-integrated differential cross-section as a function of Q^2 (squared four momentum transfer) for Δ-resonance (solid lines) and with second resonance i.e. Δ+Res2 (dotted lines) for ν-Argon (upper panel) and ν-Carbon (lower panel) with neutrino (left) and anti-neutrino (right) using GENIE (blue lines) and GiBUU (red lines).

Carbon ($\approx$ 115 MeV) for neutrino (for anti-neutrino, $\approx$ 105 MeV for both Argon and Carbon) with the inclusion of the second resonance region (Δ+Res2), as compared to the Δ resonance using GENIE. Similarly, a noticeable difference is observed using GiBUU ($\approx$160 MeV for Argon and $\approx$170 MeV for Carbon in case of neutrino while for anti-neutrino $\approx$ 145 MeV for both Argon and Carbon). The flux-integrated differential cross-section, as a function of the Q^2 (squared four-momentum transfer), for Argon and Carbon for both the neutrino and anti-neutrino mode are shown in the Fig. 4. We have noticed a similar pattern in the event distribution as the hadronic energy distribution. This is due to the explicit dependence of this kinematic variable on the reconstructed baryonic and mesonic energies.

It is clearly evident from Figs. 3 and 4 that the extended analysis of the second resonances in the event distribution has a significant variation for both Argon and Carbon targets. The $\frac{d\sigma}{dQ^2}$ distribution using GENIE for Argon target peaks at $Q^2 = 0.15$ GeV^2 for Δ-resonance only and $Q^2 = 0.25$ GeV^2 for Δ with the second resonance for neutrino, while for anti-neutrino the peak is observed at $Q^2 = 0.05$ GeV^2. In case of Carbon target, the Δ-resonance peaks at $Q^2 = 0.15$ GeV^2, while the Δ with the second resonance peaks at $Q^2 = 0.25$ GeV^2 for neutrino, $Q^2 = 0.05$ GeV^2 for Δ-resonance, and $Q^2 = 0.15$ GeV^2 for Δ with the second resonance in the anti-neutrino mode. A similar result is also observed using GiBUU for Argon target in both the neutrino and anti-neutrino mode. The same has been observed for the Carbon target in the case of neutrino, while in the anti-neutrino mode the Δ-resonance, and with the second resonance peaks at $Q^2 = 0.15$ GeV^2. This noticeable difference is due to the inclusion of the higher nucleon excitations from the second resonance region $P_{11}(1440)$, $D_{13}(1520)$, and $S_{11}(1535)$ whose subsequent decay to multiple pions contributes to the reconstructed hadronic energy. The significant difference in the flux-integrated differential cross-section of Q^2 also arises from the contribution of the total cross-sections, shown in Fig. 2, where the cross-section of the second resonance is quite sparse to the Δ-resonance but non-negligible. The compelling variation in the computed total cross-sections also reflects the differences in the neutrino and anti-neutrino interactions. The neutrino, in contrast with the anti-neutrino, is also due to the fact that the charged pions give different contributions to the energy of the final state. The individual energy spectrum of baryons (protons, neutrons) and mesons (pions) as a function of neutrino energy can be studied from the reference [53].

In order to quantify the effects of the second resonance region in Argon, we consider the ratio of the flux-integrated differential cross-section of Q^2 ($\frac{d\sigma}{dQ^2}$) distributions with the inclusion of the second resonances ($P_{11}(1440)$, $D_{13}(1520)$, $S_{11}(1535)$) to the $\Delta(1232)$ resonance for both Argon (blue lines) and Carbon (red lines) using GENIE (dashed lines) and GiBUU (dotted lines), which are shown in the Fig. 5. The left panel is for neutrino, and anti-neutrino is shown on the right panel. There is a clear distinction between the addition of the second resonance compared to the Δ-resonance alone. The flux-integrated differential cross-section $\frac{d\sigma}{dQ^2}$ ratio - (Δ+Res2)/Δ deviates from unity and increases with higher Q^2 value in GENIE while GiBUU also shows deviation from unity. We can also state that the second resonance contribution with respect to the Δ-resonance has a significant effect with the higher momentum transfer for both the neutrino and anti-neutrino.

Furthermore, to check the systematic uncertainty due to the final state interaction (FSI), we estimate the ratio of the flux-integrated differential cross-section of Q^2 ($\frac{d\sigma}{dQ^2}$) distributions for both the target viz., Argon and Carbon by considering the hN model for GENIE and switching off the final state interaction in GiBUU, and the results are shown in Fig. 6, for both the neutrino (left panel), and anti-neutrino (right panel). The differences between the FSI models for GENIE (dashed lines) are observed as Q^2

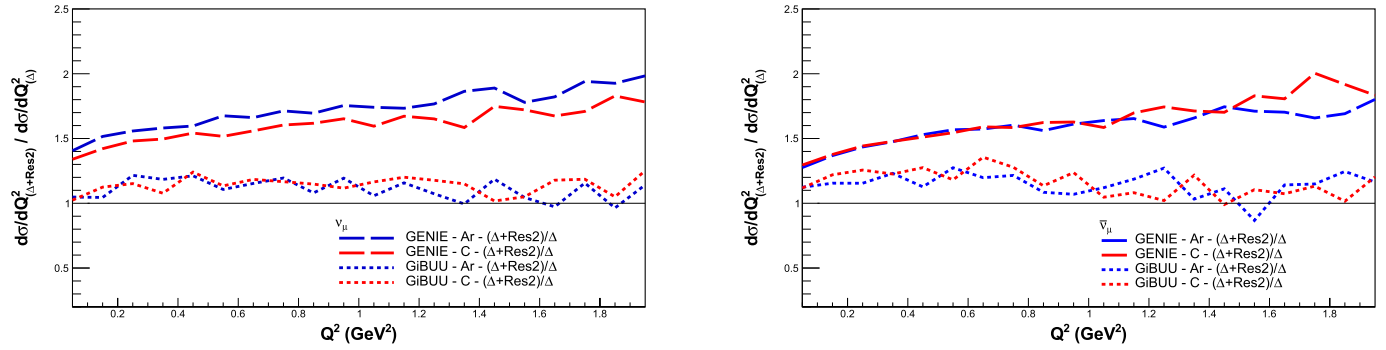

Fig. 5. The plot represents the ratio of the flux-integrated differential cross-section as a function of Q^2 (squared four momentum transfer) for Δ-resonance and with second resonance i.e. (Δ+Res2) for Argon (blue lines) and Carbon (red lines) with neutrino (left) and anti-neutrino (right) using GENIE (dashed line) and GiBUU (dotted line).

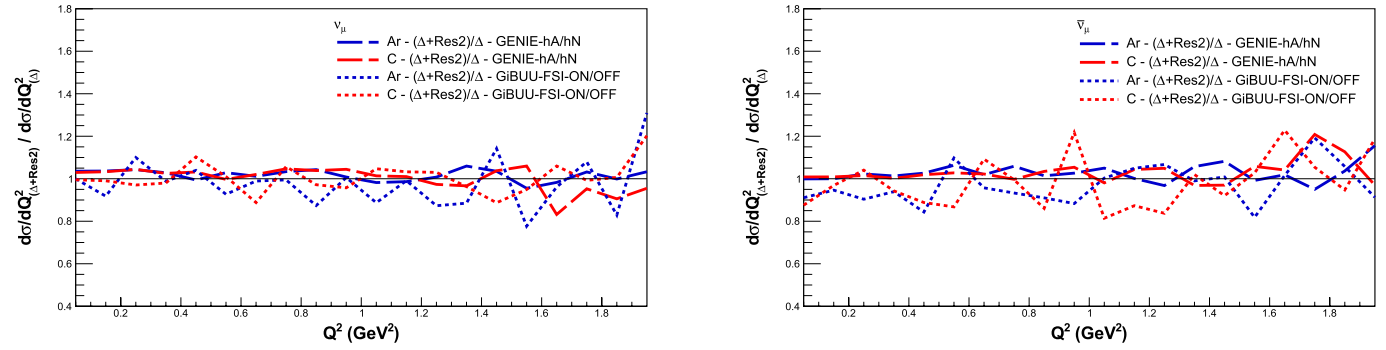

Fig. 6. The plot represents the ratio of the flux-integrated differential cross-section as a function of Q^2 (squared four momentum transfer) for Δ-resonance and with second resonance i.e. (Δ+Res2) for different FSI model for Argon (blue lines) and Carbon (red lines) with neutrino (left) and anti-neutrino (right) using GENIE (dashed line) and GiBUU (dotted line).

increases for both Argon, and Carbon target, where notable variation can be seen above $Q^2 \approx 1.6$ GeV^2 for Carbon in both the neutrino and anti-neutrino case. The effect of the FSI can also be noticed in GiBUU (dotted lines), where the anti-neutrino case evidently has larger uncertainties than the neutrino case.

5. Conclusions

The charge current neutrino interaction on nuclei has been investigated using the Monte Carlo neutrino event generator GENIE and GiBUU. We have estimated the observable for the resonance excitation by the neutrinos, and anti-neutrinos using Argon, and Carbon targets at the energy range of DUNE ND. We have found a sizable contribution from the second resonance region $P_{11}(1440)$, $D_{13}(1520)$, and $S_{11}(1535)$ for both the neutrinos and anti-neutrinos. The second resonance effect on the Argon and Carbon targets is observed using GENIE, where the Argon has slightly higher value than Carbon for all the Q^2 range in the case of neutrinos. For the anti-neutrinos, the contribution of the second resonance region is found to be higher for Carbon, above $Q^2 \approx 0.8$ GeV^2. GiBUU also shows a considerable contribution from the second resonance on the Argon, and Carbon targets in both the neutrino and anti-neutrino mode. We find from Fig. 6 that these differences are also due to the effect of the final state interaction (FSI) on different nuclear environment, which contributes to the systematic uncertainties as the inevitable nuclear effect. Thus, the excitation of higher nucleon resonances, i.e. the second resonance region has small but non-negligible effects on the cross-section measurement. The results obtained from these studies can be useful for the precision physics of the DUNE neutrino experiment as 40% of the interactions come from the resonant interaction channel at DUNE.

Declaration of competing interest

The authors declare the following financial interests/personal relationships which may be considered as potential competing interests: R Lalnuntluanga reports financial support was provided by Council of Scientific & Industrial Research (file number: 09/1001(0054)/2019-EMR-I). R Lalnuntluanga and A Giri report financial support was provided by Department of Science and Technology (SR/MF/PS-01/2016-IITH/G).

Data availability

No data was used for the research described in the article.

Acknowledgements

RL would like to thank CSIR, Government of India for the fellowship (file number: 09/1001(0054)/2019-EMR-I). RL and AG would like to thank DST, Government of India for the financial support through SR/MF/PS-01/2016-IITH/G. We thank Prof. Ulrich Mosel for useful discussions in using GiBUU.

References

[1] M. Acero, P. Adamson, L. Aliaga, T. Alion, V. Allakhverdian, S. Altakarli, N. Anfimov, A. Antoshkin, A. Aurisano, A. Back, et al., First measurement of neutrino oscillation parameters using neutrinos and antineutrinos by NOvA, Phys. Rev. Lett. 123 (15) (oct 2019), https://doi.org/10.1103/physrevlett.123.151803.
[2] K. Abe, et al., Constraint on the matter–antimatter symmetry-violating phase in neutrino oscillations, Nature 580 (7803) (2020) 339–344, Erratum: Nature 583 (2020) E16, https://doi.org/10.1038/s41586-020-2177-0, arXiv:1910.03887.
[3] B. Abi, et al., Deep Underground Neutrino Experiment (DUNE), Far Detector Technical Design Report, Volume II: DUNE Physics, 2 2020, arXiv:2002.03005.
[4] H.-K. Proto-Collaboration, K. Abe, et al., Hyper-Kamiokande design report, 2018, https://doi.org/10.48550/arxiv.1805.04163.

[5] C. Anderson, et al., First measurements of inclusive muon neutrino charged current differential cross sections on argon, Phys. Rev. Lett. 108 (2012) 161802, https://doi.org/10.1103/PhysRevLett.108.161802.

[6] R. Acciarri, et al., Measurements of inclusive muon neutrino and antineutrino charged current differential cross sections on argon in the numi antineutrino beam, Phys. Rev. D 89 (2014) 112003, https://doi.org/10.1103/PhysRevD.89.112003.

[7] K. Abe, et al., Measurement of the neutrino-oxygen neutral-current interaction cross section by observing nuclear deexcitation γ rays, Phys. Rev. D 90 (2014) 072012, https://doi.org/10.1103/PhysRevD.90.072012.

[8] K. Abe, et al., First measurement of the muon neutrino charged current single pion production cross section on water with the t2k near detector, Phys. Rev. D 95 (2017) 012010, https://doi.org/10.1103/PhysRevD.95.012010.

[9] K. Abe, et al., Measurement of the inclusive ν_μ charged current cross section on iron and hydrocarbon in the t2k on-axis neutrino beam, Phys. Rev. D 90 (2014) 052010, https://doi.org/10.1103/PhysRevD.90.052010.

[10] B.G. Tice, et al., Measurement of ratios of ν_μ charged-current cross sections on C, Fe, and Pb to CH at neutrino energies 2–20 gev, Phys. Rev. Lett. 112 (2014) 231801, https://doi.org/10.1103/PhysRevLett.112.231801.

[11] O. Lalakulich, U. Mosel, K. Gallmeister, Neutrino energy reconstruction in quasielastic-like scattering in the MiniBooNE and T2K experiments, Phys. Rev. C 86 (2012) 054606, https://doi.org/10.1103/PhysRevC.86.054606.

[12] J. Singh, S. Nagu, J. Singh, R. Singh, Quantifying multinucleon effect in argon using high-pressure tpc, Nucl. Phys. B 957 (2020) 115103, https://doi.org/10.1016/j.nuclphysb.2020.115103.

[13] C. Andreopoulos, A. Bell, D. Bhattacharya, F. Cavanna, J. Dobson, S. Dytman, H. Gallagher, P. Guzowski, R. Hatcher, P. Kehayias, A. Meregaglia, D. Naples, G. Pearce, A. Rubbia, M. Whalley, T. Yang, The GENIE neutrino Monte Carlo generator, Nucl. Instrum. Methods Phys. Res., Sect. A, Accel. Spectrom. Detect. Assoc. Equip. 614 (1) (2010) 87–104, https://doi.org/10.1016/j.nima.2009.12.009.

[14] O. Buss, T. Gaitanos, K. Gallmeister, H. van Hees, M. Kaskulov, O. Lalakulich, A. Larionov, T. Leitner, J. Weil, U. Mosel, Transport-theoretical description of nuclear reactions, Phys. Rep. 512 (1) (2012) 1–124, https://doi.org/10.1016/j.physrep.2011.12.001.

[15] T. Golan, J.T. Sobczyk, J. Zmuda, NuWro: the Wroclaw Monte Carlo generator of neutrino interactions, Nucl. Phys. B, Proc. Suppl. 229–232 (2012) 499, https://doi.org/10.1016/j.nuclphysbps.2012.09.136.

[16] Y. Hayato, L. Pickering, The NEUT neutrino interaction simulation program library, Eur. Phys. J. Spec. Top. (2021) 1–13, https://doi.org/10.1140/epjs/s11734-021-00287-7.

[17] D. Drakoulakos, et al., Minerva Collaboration, Repor. No. FERMILAB-PROPOSAL-0938, 2004.

[18] M. Antonello, et al., A Proposal for a Three Detector Short-Baseline Neutrino Oscillation Program in the Fermilab Booster Neutrino Beam, 3 2015, arXiv:1503.01520.

[19] Y. Fukuda, et al., The Super-Kamiokande detector, Nucl. Instrum. Methods Phys. Res., Sect. A, Accel. Spectrom. Detect. Assoc. Equip. 501 (2003) 418–462, https://doi.org/10.1016/S0168-9002(03)00425-X.

[20] K. Duffy, High-pressure gaseous argon TPC for the DUNE near detector, in: Meeting of the Division of Particles and Fields of the, American Physical Society, 2019, arXiv:1910.06422.

[21] O. Lalakulich, E.A. Paschos, G. Piranishvili, Resonance production by neutrinos: the second resonance region, Phys. Rev. D 74 (1) (jul 2006), https://doi.org/10.1103/physrevd.74.014009.

[22] E. Vagnoni, O. Benhar, D. Meloni, Inelastic neutrino-nucleus interactions within the spectral function formalism, Phys. Rev. Lett. 118 (14) (apr 2017), https://doi.org/10.1103/physrevlett.118.142502.

[23] E. Vagnoni, Theoretical description and reconstruction of neutrino interactions, and systematic uncertainties of long-baseline oscillation experiments, Ph.D. thesis, 2016.

[24] D.T. Agudelo, A. Mariano, D.J. Arango, Weak pion-production and the second resonance region, Phys. Rev. D 105 (3) (feb 2022), https://doi.org/10.1103/physrevd.105.033008.

[25] E. Wang, L. Alvarez-Ruso, J. Nieves, Photon emission in neutral-current interactions at intermediate energies, Phys. Rev. C 89 (1) (jan 2014), https://doi.org/10.1103/physrevc.89.015503.

[26] E.A. Paschos, J.-Y. Yu, M. Sakuda, Neutrino production of resonances, Phys. Rev. D 69 (2004) 014013, https://doi.org/10.1103/PhysRevD.69.014013.

[27] S. Manly, M. Kordosky, et al., D. Collaboration, Deep underground neutrino experiment (DUNE) near detector conceptual design report, Instruments 5 (4) (2021) 31.

[28] P. Adamson, et al., Study of muon neutrino disappearance using the fermilab main injector neutrino beam, Phys. Rev. D 77 (2008) 072002, https://doi.org/10.1103/PhysRevD.77.072002.

[29] H. Chen, et al., Proposal for a New Experiment Using the Booster and NuMI Neutrino Beamlines: MicroBooNE, FERMILAB-PROPOSAL-0974, 2007.

[30] LBNE Collaboration, C. Adams, D. Adams, T. Akiri, T. Alion, K. Anderson, C. Andreopoulos Andrews, et al., The long-baseline neutrino experiment: exploring fundamental symmetries of the universe, https://doi.org/10.48550/ARXIV.1307.7335, 2013.

[31] A. Bodek, J.L. Ritchie, Further studies of Fermi-motion effects in lepton scattering from nuclear targets, Phys. Rev. D 24 (1981) 1400–1402, https://doi.org/10.1103/PhysRevD.24.1400.

[32] J. Nieves, I. Ruiz Simo, M. Vicente Vacas, The nucleon axial mass and the miniboone quasielastic neutrino–nucleus scattering problem, Phys. Lett. B 707 (1) (2012) 72–75, https://doi.org/10.1016/j.physletb.2011.11.061, https://www.sciencedirect.com/science/article/pii/S0370269311014407.

[33] J. Nieves, J.E. Amaro, M. Valverde, Inclusive quasi-elastic neutrino reactions, Phys. Rev. C 70 (2004) 055503, Erratum: Phys. Rev. C 72 (2005) 019902, https://doi.org/10.1103/PhysRevC.70.055503, arXiv:nucl-th/0408005.

[34] R. Gran, J. Nieves, F. Sanchez, M.J.V. Vacas, Neutrino-nucleus quasi-elastic and 2p2h interactions up to 10 gev, Phys. Rev. D 88 (2013) 113007, https://doi.org/10.1103/PhysRevD.88.113007, https://link.aps.org/doi/10.1103/PhysRevD.88.113007.

[35] C. Llewellyn Smith, Neutrino reactions at accelerator energies, Phys. Rep. 3 (5) (1972) 261–379, https://doi.org/10.1016/0370-1573(72)90010-5.

[36] O. Lalakulich, K. Gallmeister, U. Mosel, Many-body interactions of neutrinos with nuclei - observables, Phys. Rev. C 86 (1) (2012) 014614, Erratum: Phys. Rev. C 90 (2014) 029902, https://doi.org/10.1103/PhysRevC.86.014614, arXiv:1203.2935.

[37] R. Bradford, A. Bodek, H. Budd, J. Arrington, A new parameterization of the nucleon elastic form factors, in: Proceedings of the 4th International Workshop on Neutrino-Nucleus Interactions in the Few-GeV Region, Nucl. Phys. B, Proc. Suppl. 159 (2006) 127–132, https://doi.org/10.1016/j.nuclphysbps.2006.08.028.

[38] A. Bodek, S. Avvakumov, R. Bradford, H.S. Budd, Vector and axial nucleon form factors: a duality constrained parameterization, Eur. Phys. J. C 53 (2008) 349–354, https://doi.org/10.1140/epjc/s10052-007-0491-4, arXiv:0708.1946.

[39] T. Katori, Meson Exchange Current (MEC) Models in Neutrino Interaction Generators, AIP Conference Proceedings, vol. 1663, AIP Publishing LLC, 2015, p. 030001.

[40] C. Berger, L.M. Sehgal, Lepton mass effects in single pion production by neutrinos, Phys. Rev. D 76 (2007) 113004, https://doi.org/10.1103/PhysRevD.76.113004.

[41] D. Rein, L.M. Sehgal, Neutrino-excitation of baryon resonances and single pion production, Ann. Phys. 133 (1) (1981) 79–153.

[42] D. Drechsel, O. Hanstein, S.S. Kamalov, L. Tiator, A unitary isobar model for pion photoproduction and electroproduction on the proton up to 1-GeV, Nucl. Phys. A 645 (1999) 145–174, https://doi.org/10.1016/S0375-9474(98)00572-7, arXiv:nucl-th/9807001.

[43] K.S. Kuzmin, V.V. Lyubushkin, V.A. Naumov, Axial masses in quasielastic neutrino scattering and single-pion neutrinoproduction on nucleons and nuclei, https://doi.org/10.48550/ARXIV.HEP-PH/0606184, 2006.

[44] K.S. Kuzmin, V.V. Lyubushkin, V.A. Naumov, Lepton polarization in neutrino nucleon interactions, Mod. Phys. Lett. A 19 (2004) 2815–2829, https://doi.org/10.1142/S0217732304016172, arXiv:hep-ph/0312107.

[45] L. Alvarez-Ruso, et al., Recent highlights from GENIE v3, Eur. Phys. J. Spec. Top. 230 (24) (2021) 4449–4467, https://doi.org/10.1140/epjs/s11734-021-00295-7, arXiv:2106.09381.

[46] M. Kabirnezhad, Single pion production in neutrino-nucleon interactions, Phys. Rev. D 97 (2018) 013002, https://doi.org/10.1103/PhysRevD.97.013002.

[47] A. Bodek, U. Yang, Higher twist, ξw scaling, and effective LO PDFs for lepton scattering in the few GeV region, J. Phys. G, Nucl. Part. Phys. 29 (8) (2003) 1899, https://doi.org/10.1088/0954-3899/29/8/369, arXiv:hep-ex/0210024.

[48] O. Lalakulich, K. Gallmeister, U. Mosel, Neutrino nucleus reactions within the GiBUU model, J. Phys. Conf. Ser. 408 (2013) 012053, https://doi.org/10.1088/1742-6596/408/1/012053, arXiv:1110.0674.

[49] S. Dytman, Final state interactions in neutrino-nucleus experiments, Acta Phys. Pol. B 40 (2009) 2445–2460.

[50] S. Dytman, A. Meyer, Final State Interactions in GENIE, AIP Conference Proceedings, vol. 1405, American Institute of Physics, 2011, pp. 213–218.

[51] S. Mashnik, A. Sierk, K. Gudima, M. Baznat, CEM03 and LAQGSM03—New Modeling Tools for Nuclear Applications, Journal of Physics: Conference Series, vol. 41, IOP Publishing, 2006, p. 037.

[52] P. Coloma, P. Huber, C.-M. Jen, C. Mariani, Neutrino-nucleus interaction models and their impact on oscillation analyses, Phys. Rev. D 89 (2014) 073015, https://doi.org/10.1103/PhysRevD.89.073015.

[53] A.M. Ankowski, O. Benhar, P. Coloma, P. Huber, C.-M. Jen, C. Mariani, D. Meloni, E. Vagnoni, Comparison of the calorimetric and kinematic methods of neutrino energy reconstruction in disappearance experiments, Phys. Rev. D 92 (2015) 073014, https://doi.org/10.1103/PhysRevD.92.073014.

[54] A.M. Ankowski, P. Coloma, P. Huber, C. Mariani, E. Vagnoni, Missing energy and the measurement of the CP-violating phase in neutrino oscillations, Phys. Rev. D 92 (2015) 091301, https://doi.org/10.1103/PhysRevD.92.091301.

[55] M.A. Acero, et al., Adjusting neutrino interaction models and evaluating uncertainties using NOvA near detector data, Eur. Phys. J. C 80 (12) (2020) 1119, https://doi.org/10.1140/epjc/s10052-020-08577-5, arXiv:2006.08727.

[56] G.M. Radecky, et al., Study of single pion production by weak charged currents in low-energy neutrino d interactions, Phys. Rev. D 25 (1982) 1161–1173, Erratum: Phys. Rev. D 26 (1982) 3297, https://doi.org/10.1103/PhysRevD.25.1161.

[57] D. Rein, L.M. Sehgal, PCAC and the deficit of forward muons in π^+ production by neutrinos, Phys. Lett. B 657 (2007) 207–209, https://doi.org/10.1016/j.physletb.2007.10.025, arXiv:hep-ph/0606185.

[58] A.V. Butkevich, Analysis of flux-integrated cross sections for quasi-elastic neutrino charged-current scattering off ^{12}C at energies available at the MiniBooNE experiment, Phys. Rev. C 82 (2010) 055501, https://doi.org/10.1103/PhysRevC.82.055501.

[59] L. Alvarez-Ruso, et al., NuSTEC white paper: status and challenges of neutrino–nucleus scattering, Prog. Part. Nucl. Phys. 100 (2018) 1–68, https://doi.org/10.1016/j.ppnp.2018.01.006, arXiv:1706.03621.

[60] J. Martin-Albo, A pressurized argon gas TPC as DUNE near detector, J. Phys. Conf. Ser. 888 (1) (2017) 012154, https://doi.org/10.1088/1742-6596/888/1/012154, arXiv:1610.07803.

[61] B. Abi, et al., Experiment simulation configurations approximating DUNE TDR, arXiv:2103.04797, 3 2021.

[62] T.A. Mohayai, MPD multi-π exclusive samples, https://indico.fnal.gov/event/23441/contributions/72334/attachments/45299/54520/2020_02_24_tmohayai_2.pdf, 2020.